CHEMISTRY OF MATERIALS

Article

pubs.acs.org/cm

Preparation of High Concentration Dispersions of Exfoliated MoS_2 with Increased Flake Size

Arlene O'Neill, Umar Khan, and Jonathan N Coleman*

School of Physics and CRANN, Trinity College Dublin, Dublin 2, Ireland

ABSTRACT: Solvent exfoliation of inorganic layered compounds is likely to be important for a range of applications. However, this method generally gives dispersions of small nanosheets at low concentrations. Here we describe methods, based on sonication of powdered MoS_2 in the solvent N-methyl-pyrrolidone, to prepare dispersions with significantly increased lateral nanosheet size and dispersed concentration. We find the concentration to scale linearly with starting MoS_2 mass allowing the definition of a yield. This yield can be increased to ~40% by controlling the sonication time, resulting in concentrations as high as 40 mg/mL. We find the nanosheet size to increase initially with sonication time reaching ~700 nm (for a concentration of ~7.5 mg/mL). At longer sonication times the nanosheets size falls off due to sonication induced scission. The nanosheets produced by such methods are relatively thin and have no observable defects. We can separate the dispersed nanosheets by size using controlled centrifugation. This allows us to produce dispersions with mean flake size of up to ~2 μm. However, such large flakes are noticeably thicker than the standard nanosheets. We demonstrate that such nanosheets can be mixed with polymers to form composites. While standard nanosheets result in no improvement in composite mechanical properties, addition of size-selected nanosheets results in significant improvements in composite modulus and strength.

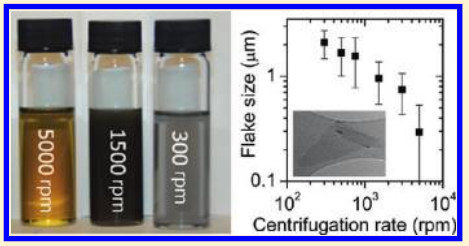

KEYWORDS: *layered compound, exfoliation, two-dimensional, dispersion, nanosheets, composite*

INTRODUCTION

Two dimensional (2D) nanosheets are a new class of materials which are expected to become important for a range of applications. Although graphene is probably the best known 2D material,[1] a wide range of others exist,[2] with BN and MoS_2 the most studied. Under normal circumstances, nanosheets stack together in layered crystals. However as with graphene,[3] a number of researchers have found that individual inorganic nanosheets can be removed from their parent crystal by micromechanical cleavage.[3−10] This has allowed the structural characterization of BN by high resolution TEM[4] and its use as a substrate for high performance graphene devices.[11] Similarly, for MoS_2 a number of advances have been demonstrated including the production of sensors,[12] transistors,[3,9,13] and integrated circuits,[10] the measurement of the mechanical properties of individual nanosheets[8] and the observation of the evolution of the vibrational[5] and electronic structure[6,7] with number of stacked nanosheets.

However, a number of applications exist where nanosheets will be required in large quantities. For example, the impressive mechanical properties[8,14,15] of BN and MoS_2 make them attractive as fillers to reinforce plastics. Thin films prepared from exfoliated MoS_2 and γ-MnO_2 are promising as electrodes in lithium ion batteries[16−18] and supercapcacitors[19−21] respectively. In addition, the exfoliation of layered compounds may lead to the development of efficient thermoelectric devices.[18,22] To produce enough exfoliated material for such applications, a scalable production method is required. By analogy with the development of liquid exfoliation of graphene[23] and graphene oxide,[24] access to a similar processing methods will advance the development of other 2D materials.

We note that liquid phase methods to exfoliate transition metal dichalcogenides (TMDs) and transition metal oxides (TMOs) using ion intercalation have been known since the 1980s[25−27] and are experiencing something of a revival today.[28,29] However, such methods are time-consuming, extremely sensitive to environmental conditions and are relatively ineffective for selenides and tellurides. In addition, ion intercalation results in structural deformations in some TMDs.[30] While the pristine structure can be recovered by annealing the nanosheets in thin film form,[28] we feel that the disadvantages associated with these methods are significant.

However, recently it has been shown that both BN[22,31−35] and TMDs[18,22,36,37] can be exfoliated in liquids (solvents or aqueous surfactant solutions) without any of the problems described above. Briefly, exfoliation in liquids involves the mechanical exfoliation of layered crystals by ultrasonication in an appropriate liquid. The exfoliated nanosheets then tend to be stabilized against reaggregation either by interaction with the solvent or through electrostatic repulsion due to the adsorption of surfactant molecules.[38] In the case of solvent stabilization, it has been shown that good solvents are those where the surface energy of solvent and nanosheets match. This results in the enthalpy of mixing being very small.[22,37] Because these exfoliation methods are based on van der Waals interactions between the nanosheets and either the solvent molecules or

Received: May 16, 2012
Published: May 29, 2012

   dx.doi.org/10.1021/cm301515z | *Chem. Mater.* 2012, 24, 2414−2421

surfactant tail group, stabilization does not result in any significant perturbation of the properties of the nanosheet. These dispersions can easily be formed into films or composites[18,22] and facilitate processing for a wide range of applications.

However, these methods have three main shortcomings. Both solvent-[22] and surfactant-exfoliated[18] TMDs tend to exist as multilayer stacks with few individual nanosheets. This is in contrast to ion exfoliation methods which give reasonably large monolayer populations.[28] Second, the dispersed concentrations tend to be well below 1 mg/mL, too low for applications requiring large quantities of exfoliated material. Finally, the lateral flake size is relatively small, typically 200−400 nm. This is probably due to sonication induced scission and limits the potential of these materials in a range of applications from composites to transistors or sensors.

Thus, it will be important to find ways to modify solvent (and surfactant) exfoliation methods to improve the exfoliation state (i.e., decrease the average flake thickness) and increase both the dispersed concentration and the flake size. In this paper, we address two of these problems. We show that the sonication conditions can be controlled to give relatively large flakes at relatively high concentration. In addition, we show that the flakes can be further size selected to give dispersions with a range of mean flake sizes.

EXPERIMENTAL SECTION

The MoS_2 powder and NMP used throughout these experiments were purchased from Sigma Aldrich (CAS 69860 and CAS M79603). The initial MoS_2 concentration experiments were performed by adding the powder to 20 mL of NMP in a 100 mL capacity, flat bottomed beaker. These samples were sonicated continuously for 60 min using a horn probe sonic tip (VibraCell CVX, 750W, 25% amplitude). The beaker was connected to a cooling system that allowed for cold water (5 °C) to flow around the dispersion during sonication. They were then centrifuged using a Hettich Mikro 22R at 1500 rpm for 45 min. Absorption spectroscopy measurement were performed using a Cary 6000i and a 1 cm cuvette. For the concentration versus sonication time experiments, 100 mL of NMP was added to 10 g of MoS_2. The sonic tip was pulsed for 8 s on and 2 s off to avoid damage to the processor and reduce solvent heating and thus degradation. During sonication 5 mL aliquots were removed at certain time intervals and centrifuged. Bright field transmission electron microscopy imaging was performed using a JEOL 2100 (200 kV). All samples were diluted and prepared by pipetting a few mls of the dispersion onto the holey carbon grid (400 mesh) purchased from Agar Scientific. Statistical analyses (N = 50) of the flake dimensions were performed by measuring the longest axis of the flake and recording it as its length, and the axis perpendicular to this at the widest point, as its width. High resolution imaging of the flakes was performed using an FEI Titan TEM (300 kV). Flake size separation by centrifugation was performed using a Thermo Scientific, Heraeus, Megafuge 16 centrifuge.

Nanosheet dispersions were prepared for composite formation in two ways. First we prepared nanosheets by a standard processing method (t_{sonic} = 50 h, no size selection). These flakes were relatively small ($\langle L \rangle \geq 0.7$ μm). Second we used size selected flakes (t_{sonic} = 50 h, final rotation rate 300 rpm for 45 min) $\langle L \rangle \geq 2$ μm). To remove the NMP, the dispersions were diluted by a factor of 30 in isopropanol (IPA), and bath sonicated for 10 min. This allowed filtration of the dispersion through a nitrocellulose membrane (Millipore, 0.02 μm pore size, 47 mm diameter). After filtration the MoS_2 coated membrane was sonicated for 10 min in water, after which the membrane was removed and its concentration measured by absorption spectroscopy. These dispersions were added to PVA/water (30 mg/mL) such that the MoS_2/PVA mass ratio was 0.25 wt %. This is equivalent to a volume fraction of 0.065 vol %, taking polymer and MoS_2 densities as 1300 and 5000 kg/m^3. The composite dispersions were sonicated for 4 h in a sonic bath (Branson 1510E-MT). The dispersions were then drop-cast into Teflon trays and dried overnight at 60 °C followed by further drying at 80 °C for 4 h. A polymer only film was prepared using a similar procedure. The films were cut into strips of dimensions 20 mm ×2.25 mm ×30 μm using a die cutter and tested mechanically using a Zwick Z100 tensile tester with a 100 N load cell at strain rate of 15 mm/min. For each material, five strips were measured.

RESULTS AND DISCUSSION

Maximization of Concentration. To maximize the concentration of dispersed MoS_2, it will be necessary to optimize the dispersion parameters. We focus on the solvent *N*-methyl-pyrrolidone (NMP) because it is known to be an excellent solvent, not only for MoS_2,[22,37] but also for carbon nanotubes[39] and graphene.[23,40] To begin, we prepared dispersions, while varying the initial concentration (C_I) of MoS_2 powder from 5 to 200 mg/mL (in 20 mL of solvent). The dispersions were probe sonicated for 60 min and then centrifuged at 1500 rpm to remove any unexfoliated material. The supernatant was decanted and their optical absorption spectra were measured (Figure 1A). The spectra consist of an

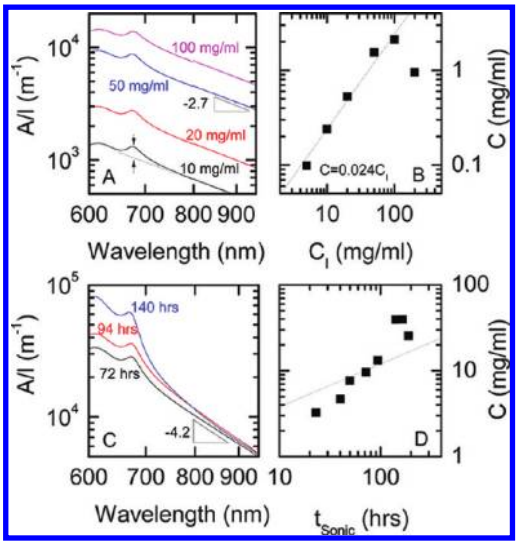

Figure 1. Dispersion of MoS_2 at high concentration. (A) Absorption spectra of MoS_2 dispersions prepared with various starting concentrations. Note that each spectrum is superimposed on a scattering background. The concentration was estimated from the absorbance above an extrapolated background as shown by the arrows using an absorption coefficient of 1020 mL/mg/m. (B) Dispersed concentration as a function of initial MoS_2 concentration. The dashed line shows the initial linear increase. (C) Absorbance spectra for various sonication times. Note that the background appears to vary with sonication time. (D) Dispersed concentration as a function of sonication time. The dashed line illustrates $\sqrt{t_{sonic}}$ behavior.

excitonic feature at 679 nm and other resonant features at lower wavelength superimposed on a power law scattering background ($\propto \lambda^{-n}$). It was immediately clear that, although the scattering exponent, n, was roughly constant, the overall magnitude of the absorbance varied considerably with C_I. Because the scattering exponent, n, is thought to depend on flake size,[18,22] this implies the lateral flake dimensions to be independent of initial concentration. Because of the potential for variation of n with flake size, the absolute value of absorbance per cell length (A/l) cannot, in general, be used to reliably measure the concentration. To estimate the concen-

dx.doi.org/10.1021/cm301515z | Chem. Mater. 2012, 24, 2414−2421

tration, the scattering background was extrapolated from the high-wavelength region (dashed line in Figure 1A) and the value of A/l solely due to resonant absorption, $(A/l)_R$, was estimated for each sample (679 nm, illustrated by arrows in Figure 1A). The concentration of dispersed material can be determined using $(A/l)_R$, provided the resonant absorption coefficient, α_R, is known. To measure α_R, a known volume of dispersion was filtered through a membrane. By careful weighing, the concentration, C, could be measured and α_R estimated from the measured $(A/l)_R$ $[(A/l)_R = \alpha_R C]$ to give α_R = 1020 mL/mg/m. In most cases, this allowed us to determine the concentration of MoS_2 dispersions regardless of the value of the scattering exponent. The measured concentration as a function of C_I is shown in Figure 1B to increase from $C \approx 0.1$ mg/mL for C_I = 5 mg/mL to $C \approx 2$ mg/mL for C_I = 100 mg/mL before falling off at higher initial concentrations. The initial increase is linear as indicated by the dashed line. This slope of this line gives the yield of the dispersion procedure which was 2.4% under these circumstances.

It has been reported for various nanomaterials that prolonged sonication results in increased dispersion concentrations.[40,41] To test if this applies to MoS_2, 100 mL of NMP was added to 10 g of MoS_2 (C_I = 100 mg/mL) in a beaker and probe sonicated for up to ~200 h. At various time intervals aliquots were removed, centrifuged (1500 rpm, 45 min), decanted, and the absorption spectrum recorded (Figure 1C). In this case the scattering exponent was not constant, increasing from n = 2.7 to n = 4.2 as the sonication time was increased, suggesting a variation in flake size.[18] The concentration was determined from the spectra as before and is plotted as a function of sonication time in Figure 1D. The concentration increased from 3.2 mg/mL after 23 h sonication to 40 mg/mL after 140 h before falling off slightly. These concentrations are extremely high and compare favorable to the highest concentration graphene dispersions.[42] We note that the highest concentration achieved implies a yield of 40% demonstrating the efficiency of this dispersion process. However, unlike the situation for graphene,[40,41] the concentration of the dispersion does not scale well with the square root of sonication time (illustrated by the dotted line in Figure 1D). This suggests the exfoliation kinetics may vary between layered materials.

The ability to produce such highly concentrated MoS_2 dispersions will be useful, provided the flake quality is preserved. To test this, a subset of dispersions was examined using transmission electron microscopy (TEM). Generally, the flakes appeared well exfoliated (Figure 2A and B) with some very thin sheets, perhaps even monolayers observed (figure 2C). Further examination of the flake quality was performed by high resolution TEM imaging (Figure 2D and E). These images illustrated that prolonged sonication did not appear to damage or disrupt the hexagonal structure of MoS_2. Unlike graphene,[40] the level of exfoliation cannot be quantified for MoS_2 by edge counting.[22] However, statistical analysis of the lateral flake dimensions (i.e., length, L and width, w) is possible. Shown in figure 2F are the mean values of L and w plotted versus sonication time. Both dimensions increase from relatively low values $[\langle L\rangle \approx 0.3\ \mu m, \langle w\rangle \approx 0.17\ \mu m]$ after 23 h sonication, to a maximum $[\langle L\rangle \approx 0.7\ \mu m, \langle w\rangle \approx 0.4\ \mu m]$ after 60 h sonication. This may reflect the preferential exfoliation of MoS_2 crystallites by size. However, after 60 h, the flake dimensions decrease, reaching $\langle L\rangle \approx 0.2\ \mu m$ and $\langle w\rangle \approx 0.15\ \mu m$ after 142 h of sonication. In the second regime the data are consistent with an inverse square root dependence with sonication time (i.e., $\propto t^{-1/2}$, dashed line). This suggests the flakes to be cut by sonication induced scission[43] as observed previously for graphene dispersions.[40]

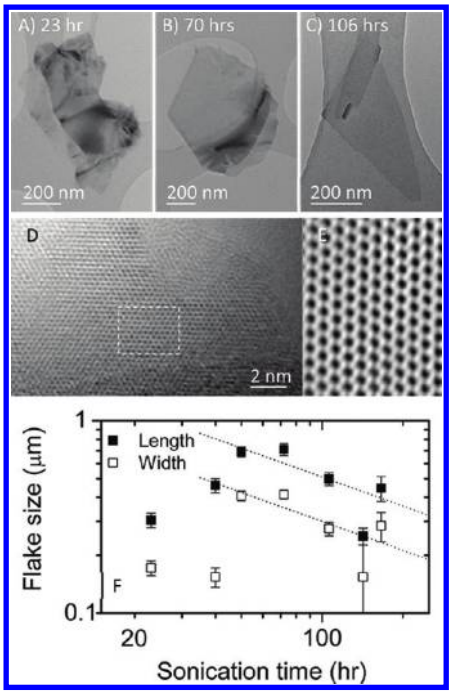

Figure 2. (A, B, and C) Sample images of MoS_2 flakes prepared with sonication times of 23, 70, and 106 h, respectively. (D) A HRTEM image of an MoS_2 flake. Note the well-defined hexagons in the dashed box. (E) A digitally filtered image of a portion of the flake within the dashed box. (F) Mean flake length and width (calculated from 50 measurements) as a function of sonication time. The dashed lines represent $1/\sqrt{t_{Sonic}}$ behavior.

Although these MoS_2 flakes are laterally larger than previously reported $[\langle L\rangle \approx 0.7\ \mu m$ compared to $\langle L\rangle \approx 0.3\ \mu m$ reported by Coleman et al. and Smith et al.$]$,[18,22] they are still smaller than the graphene flakes obtained using similar sonication and centrifugation (CF) regimes.[40,44] This may be due to two things, first the size of crystallites in the initial starting MoS_2 powder $[\langle L\rangle \approx 10\ \mu m]$, is much smaller than that of the graphite used in earlier studies $[\langle L\rangle \approx 700\ \mu m]$.[23] However, perhaps more likely, sonication induced scission should give a flake size which is determined by the material tensile strength.[45] Lucas has suggested that for rods cut by sonication induced scission, the terminal length, L_t, scales with strength, σ_B, $L_t \propto (\sigma_B)^{1/2}$.[45] While we cannot definitively state the flakes described in Figure 2F have reached their terminal size, we nevertheless compare their length after the longest sonication time (440 nm after 166 h) to graphene flakes sonicated in NMP which appear to have reached terminal length (~800 nm after 350 h).[40] Taking the known strengths of graphene and MoS_2 (130 and 23 GPa),[8,46] and applying Lucas's expression predicts $L_{t,G}/L_{t,MoS_2} = (130/23)^{1/2} = 2.4$. This is reasonably close to our estimate from the experimental data of $L_{t,G}/L_{t,MoS_2} \geq 800/440 = 1.8$ (the inequality is because the MoS_2 flakes have probably not reached terminal length). The good agreement suggests the relative flake sizes observed for graphene and MoS_2 are consistent with sonication induced scission.

Separation of Flakes by Size. Recent research has indicated that graphene flakes can be selected by size by

dx.doi.org/10.1021/cm301515z | Chem. Mater. 2012, 24, 2414−2421

controlled centrifugation coupled with sediment recycling.[47,48] To test if this could be extended to MoS_2 dispersions, an MoS_2/NMP dispersion which had been sonicated for 50 h followed by centrifugation at 1500 rpm for 45 min was selected. This dispersion was chosen based on its relatively high concentration (7.6 mg/mL) and relatively large flakes [$\langle L \rangle \approx 0.7$ μm]. To begin separating the flakes this stock dispersion was centrifuged at the high rate of 5000 rpm for 45 min (centrifugation time remained constant throughout this study). This acted to separate the smaller flakes which remained in the supernatant from the medium and larger flakes in the sediment.[44,47] After CF, 8 mL of supernatant was decanted and stored for further analysis, after which 8 mL of fresh NMP were added to the sediment in the same vial. The mixture was stirred and sonicated for 15 min before recentrifuging it at the lower rate of 3000 rpm again separating flakes by size. The supernatant was decanted and fresh NMP was once again added to the sediment. This procedure was repeated another 4 times for 1500, 750, 500, and 300 rpm. We label all samples by their final centrifugation rate. Each sample is expected to contain a well-defined size range. This can be illustrated with reference to the 1500 rpm sample for example. The final centrifugation of this dispersion (1500 rpm) removed flakes above a certain lateral size. In addition, the previous step (centrifugation at 3000 rpm followed by redispersing the sediment) had removed all flakes below a given lateral size. Thus, we expect this to be an efficient separation method. By analogy with previous work, we expect the flake size to increase as the final centrifugation rate decreases.[47] The color of the resultant dispersions varied strongly with final centrifugation rate indicating that the nature of the nanosheets had indeed changed (Figure 3A).

After each centrifugation step, we performed absorption spectroscopy. For high centrifugation rates, the spectra were superimposed on a scattering background similar to that observed previously. However for lower rotation rates the spectra had changed significantly, appearing flatter and more featureless as the rotation rate fell (figure 3B). This may be partly due to dependence of the scattering exponent on flake dimension. To test this, we estimated the scattering exponent, n, from the high wavelength region, which is plotted as a function of centrifugation rate in Figure 3B inset. The scattering exponent was close to 4 for high rotation rates. This is what might be expected for Rayleigh scattering, which would be consistent with the retention of small flakes at high CF rates.[47] In addition, the scattering exponent decreased with decreasing rotation rate, that is, with increasing flake size. However, this does not entirely describe the spectral changes; at lower rotation rates the absorption spectra appeared distorted such that background subtraction was impossible. This means that optical measurements of concentration were no longer possible after the controlled CF of the dispersions. The reasons for these distortions remain unknown.

We also performed TEM on each supernatant to determine the quality and dimension of the flakes during the controlled centrifugation regime (Figure 4A–C). The TEM micrographs illustrated that the MoS_2 was well exfoliated for high rotation rates, however as the rotation rate decreased the electron transparency of the flakes also reduced indicating an increase in flake thickness. In addition, we noticed that size-selected flakes tended to have smaller flakes adsorbed in many cases. The lateral size of the flakes could also readily be determined from these TEM micrographs as plotted in Figure 4D. After the initial 5000 rpm centrifugation the flakes had a mean length and width of $\langle L \rangle \approx 0.3$ μm and $\langle w \rangle \approx 0.15$ μm. However as the final rotation rate decreased, the flake dimensions increased, reaching $\langle L \rangle \approx 2$ μm and $\langle w \rangle \approx 1.2$ μm for the 300 rpm sample. We have also plotted the lengths of the largest flakes observed after each CF, which reached ~5 μm for the 500 rpm sample. For comparison, the mean flake length and width and the maximum flake size measured for the starting dispersion (i.e. before size selection) are indicated by the horizontal lines. Once the flake dimensions were known, we plotted the scattering exponent as a function of flake length (figure 4D, inset). Flakes with lengths below 1 μm have exponents between 3 and 4, while longer flakes have lower exponents. This is consistent with our earlier prediction that the scattering component varies with flake dimension.

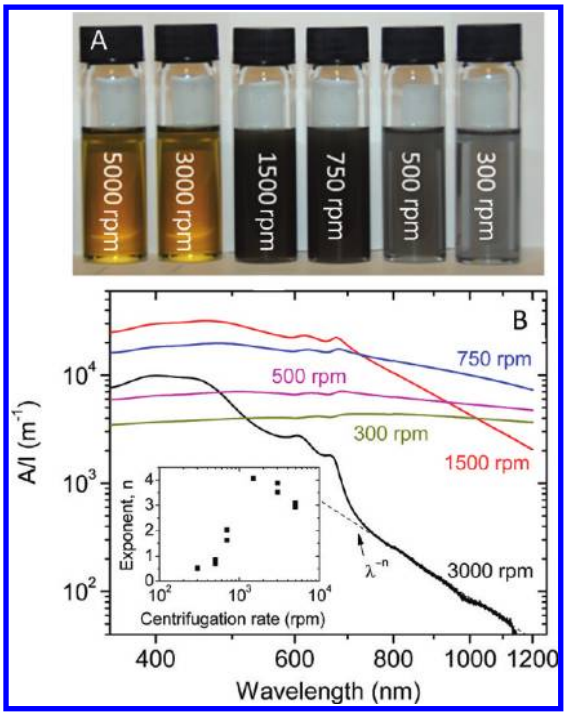

Figure 3. (A) Photograph of the dispersions after size selection (these dispersions have been diluted by a factor of 100 to emphasize the color change). (B) Absorption spectra for the dispersions in A. In both A and B, the samples are labeled by their final centrifugation rate. Note how the exponent of the scattering background changes with final centrifugation rate (inset).

We also examined the stability of these size selected dispersions by measuring the absorbance and hence concentration as a function of sedimentation time. Data were collected using a home-built sedimentation apparatus[49] over a 3 week period (figure 4E). The results indicated that small flakes, found in the 3000 rpm dispersion remained dispersed over the entire measurement period. In contrast, for the 1500 and 300 rpm samples, the concentration fell off steadily with time. Modeling the sedimentation as an exponential decay of concentration with time,[49] gave the sedimentation time constant, τ, and the percentage of stably dispersed material for each sample. The fit curves predicted that ~45% and ~22% are stable indefinitely and gave values of τ of 190 and 33 h, for the 1500 and 300 rpm samples respectively. Modeling has suggested that for sedimenting discs, the time constant scales with the lateral dimension, L, as $\tau \propto L^{-2}$.[49] To test this, we plotted τ against $\langle L \rangle^{-2}$ (as determined from statistical TEM

dx.doi.org/10.1021/cm301515z | Chem. Mater. 2012, 24, 2414–2421

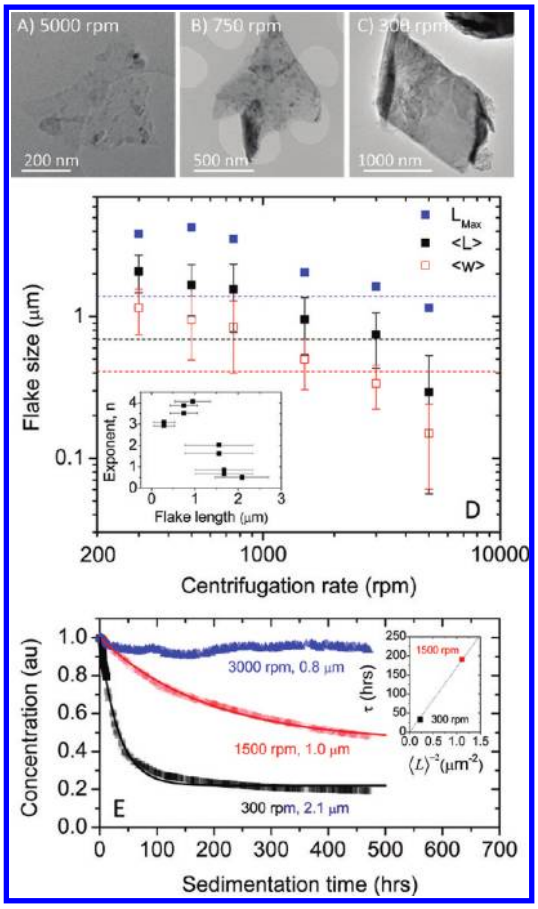

Figure 4. (A, B, and C) Sample images of flakes after size selection for different final centrifugation rates. (D) Flake size as a function of final centrifugation rate. The data points are the average of 50 measurements. Shown are data for mean flake length and width as well as the maximum flake length observed. The dashed lines represent the sizes of the flakes in the normal starting dispersion, which has been sonicated for 50 h and centrifuged once at 1500 rpm for 45 min. Inset: Scattering exponent as a function of mean flake length. (E) Concentration as a function of sedimentation time for size selected flakes of three different final centrifugation rates and mean lengths (see labels). Inset: Sedimentation time constant versus $\langle L \rangle^{-2}$, where L is the mean flake length at the start of the sedimentation experiment.

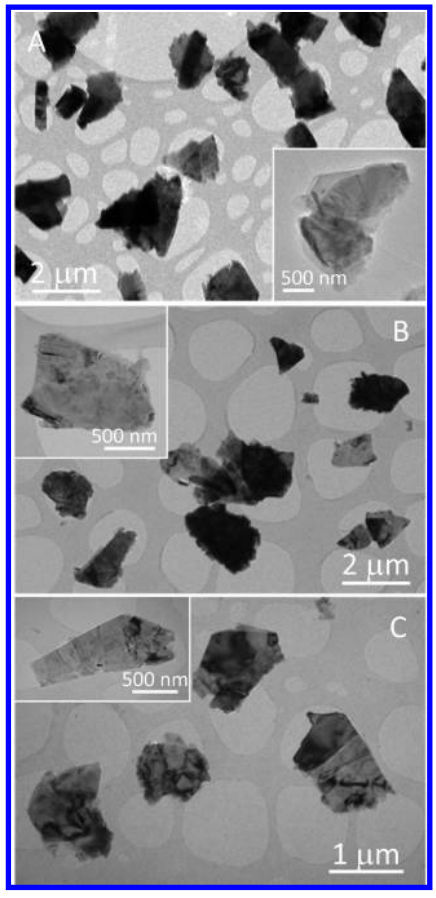

Figure 5. TEM micrographs of size selected dispersions produced by centrifugation at 300 rpm as part of (A) the normal regime, (B) the reduced centrifugation regime, and (C) the reduced centrifugation regime followed by a 100 fold dilution in NMP. The insets show examples of thinner flakes observed in each case.

analysis) finding perfect agreement (i.e., the fit line goes through the origin, figure 4E inset).

Taken together, this suggests that sedimentation occurs at a rate defined by the nanosheet size until a stable concentration is reached. This stable concentration appears to be size dependent such that higher concentrations are attainable for smaller flakes.

It is worth considering in more detail the dispersion with the largest mean flake size. Shown in figure 5A is a widefield image of a sample of the largest flakes attained (300 rpm). It is clear that most of the flakes are relatively thick. While thinner flakes were observed (inset), they only represent 10−15% of the total population.

We have confirmed that the controlled centrifugation regime successfully isolates MoS_2 flakes of different dimensions; however the process is complex and can take up to 6 h of centrifugation. In order to reduce the number of centrifugation steps, we prepared a dispersion by sonicating it for 50hrs and centrifuged it at the low rotation rate of 500 rpm with the aim of separating the larger flakes into the sediment while leaving the smaller flakes in the supernatant. The supernatant was decanted and fresh NMP was added to the sediment. The mixture was stirred and sonciated for 15 min before centrifuging it again at 300 rpm to remove any remaining large aggregates. The process was similar to before but with four fewer centrifugation steps, thus greatly reducing the experimental time. TEM imaging of the dispersions gave the flake size for this truncated size selection procedure to be $\langle L \rangle \approx 1.9$ μm and $\langle w \rangle \approx 1.2$ μm which is virtually identical to the results for the 300 rpm sample prepared by the longer procedure. A TEM image of the flakes produced by this shortened procedure is shown in Figure 5B. The flakes look very similar to the ones shown in Figure 5A. As before, most flakes are relatively thick with a small population (10−15%) relatively thin (inset).

It may be possible to explain the correlation between flake size and thickness as follows. At high concentrations, large flakes will have a relatively small solvent volume per flake. This may drive aggregation until the volume of solvent per flake increases to an appropriate level. We note that a similar phenomenon has been observed for carbon nanotubes dispersed in solvents where the aggregation state (manifested by the bundle diameter) varied reversibly as the concentration was cycled from high to low.[50,51] Solvent exfoliated graphene nanosheets appear to display similar behaviour.[40] For such a system, it has been shown that there is a relationship between the dispersed concentration, C, and mean flake dimensions for exfoliated graphene: $C \propto \langle w \rangle \langle t \rangle / \langle L \rangle^2$ (length, L, width, w, and

dx.doi.org/10.1021/cm301515z | Chem. Mater. 2012, 24, 2414−2421

thickness, t).[40] This implies that large flakes, dispersed at relatively high concentration, as is the case here, should be relatively thick. This suggests that thinner flakes might be obtained by reducing the concentration. To test this, we diluted the 300 rpm sample described above by a factor of 100 by addition of NMP followed by 30 min of probe sonication. TEM analysis (Figure 5C) suggested the flakes to be marginally thinner (higher electron transparency). However, they were also slightly smaller ($\langle L \rangle \approx 1.6$ μm and $\langle w \rangle \approx 0.9$ μm), probably as a result of the additional sonication Thus, it is not clear if dilution results in a net improvement.

However, it is worth noting that a modest increase in flake thickness may not actually be too high a price to pay for large flakes. The effect of aggregation on the electronic properties of MoS_2 is considerably different to the situation for graphene. In graphene, the electronic properties depend sensitively on the number of layers per flake (for flakes with <5 layers).[1] However, for MoS_2, the effect is considerably less significant. It is true that a large change occurs going from monolayer to bilayer; the bandgap goes from being direct with size ~1.9 eV to indirect with size of 1.6 eV.[6] However, as the number of layers is increased beyond 2, the properties change slowly; going from two to six layers, the bandgap changes from 1.6 to 1.4 eV.[6] Increasing to infinity (bulk) changes the bandgap only to 1.3 eV.[6] In all cases multilayers have indirect bandgap. This means the electronic properties of MoS_2 multilayers are relatively insensitive to flake thickness. It is unlikely that the thickness increases observed during the size selection procedure result in changes in bandgap by more than 0.1 to 0.2 eV.

MoS_2/Polymer Composites. We believe that production of high concentration dispersions of inorganic nanosheets with the potential to select by lateral size will facilitate a range of applications. Here, we demonstrate the utility of these techniques for one particular application; mechanical reinforcement of polymers. It has long been known that stiff, strong platelets have the ability to reinforce plastics. It was recently shown that individual MoS_2 monolayers have relatively high values of both stiffness, Y, and tensile strength, σ_B ($Y \approx 300$ GPa, $\sigma_B = 23$ GPa).[8,15] These values are lower than graphene ($Y = 1000$ GPa, $\sigma_B = 130$ GPa)[46] but considerably higher than macroscopic materials such as steel ($Y \approx 200$ GPa, $\sigma_B \approx 1$ GPa). However, to achieve significant reinforcement, the flakes must have lateral sizes which are large enough such that appreciable stress can be transferred from polymer matrix to filler.[48,52] In order words, large flakes are required. To test this idea, we prepared composites of MoS_2 nanosheets embedded in the polymer polyvinyl alcohol (PVA, see methods), a polymer which is commonly used as a model matrix for nanocomposite studies.[53−55] We used two types of nanosheets. First we prepared nanosheets by a standard processing method (t_{sonic} = 50 h, no size selection). These flakes were relatively small ($\langle L \rangle$ = 0.7 μm). Second we used size selected flakes (t_{sonic} = 50 h, final rotation rate 300 rpm for 45 min) $\langle L \rangle$ = 2 μm). Representative stress strain curves for a PVA-only film and composites containing 0.25 wt % (0.065 vol %) standard and size selected nanosheets are shown in Figure 6. It is clear from these curves that addition of the standard sized flakes actually degrades the mechanical properties of the PVA, while the larger flakes improve the performance. Equivalent measurements were done on five films for each sample type. In each case, the stiffness, tensile strength and strain at break were measured and the averages computed. These data are shown in Table 1. Compared to the polymer film, both strength, and modulus fell by a factor of 2 for the standard flakes but increased by ~15% for the larger flakes. Interestingly, the strain at break was unaffected by the standard flakes but doubled on addition of the larger flakes. This clearly shows that there are applications where flake size is critical.

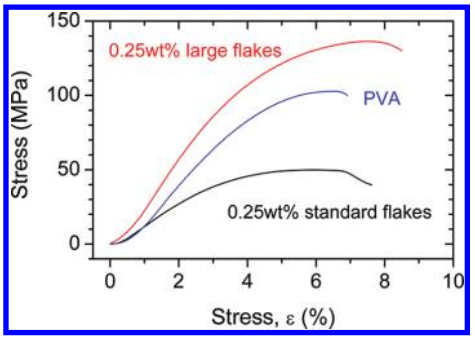

Figure 6. Mechanical properties of composites of polyvinyl alcohol (PVA) filled with 0.25 wt % MoS_2 flakes produced by the standard method (black) and 0.25 wt % size selected (large) flakes (red). The stress strain curve of a PVA film is shown for comparison.

Table 1. Mechanical Properties of Thin Films of Polyvinylalcohol (PVA) and MoS_2/PVA Composites Filled with 0.25 wt % of Normal Sized and Size Selected (Large) Flakes

	weight	Y (GPa)	UTS (MPa)	strain (%)
PVA	0	2.8 ± 0.33	108 ± 20	6 ± 1
normal flakes	0.25	1.6 ± 0.15	51 ± 8	7 ± 4
large flakes	0.25	3.2 ± 0.2	127 ± 4	11 ± 6

We can compare these results to those previously reported for large ($L \approx 2$ μm) graphene flakes in PVA.[48] There, from pure polymer to the 0.065 vol % composite the modulus increased from 3.0 to 3.4 GPa, while the strength increased from 105 to 119 MPa. These increases of 13% and 14% are remarkably similar to those found here. This implies that MoS_2 may have potential as a filler to mechanically reinforce polymers.

CONCLUSIONS

In conclusion, we have studied the effect of processing parameters on the dispersion and exfoliation of MoS_2 in the solvent NMP. We find the dispersed concentration is maximized for an initial MoS_2 concentration of 100 mg/mL. The dispersed concentration can be increased to ~40 mg/mL by increasing the sonication time to 200 h. However, the lateral flake size peaks at $\langle L \rangle \approx 700$ nm after 60 h after which it falls off because of sonication induced scission. These dispersions generally contain relatively broad flake size distributions. Such dispersions can be separated in fractions with different mean size by controlled centrifugation. Using this technique, it was possible to prepare samples with mean flake length of ~2 μm and maximum length of 4−5 μm. However, larger flakes tend to be thicker than smaller ones, a factor that can be mitigated slightly by dilution and sonication. We have shown that MoS_2 flakes can be used to reinforce plastics as long as the flakes are large enough.

We consider the results described in this work to be a significant advance. Layered compounds are an exciting class of materials with the potential to be used in a host of applications. Currently, production is the bottleneck which limits progress. We believe that liquid phase exfoliation of MoS_2 will prove to

dx.doi.org/10.1021/cm301515z | Chem. Mater. 2012, 24, 2414−2421

be a valuable production method which can produce flakes for a number of applications. However, it is undoubtedly true that high dispersed concentrations and large flakes will be necessary for many if not most applications. In this paper we have described methods to produce such properties. While we have concentrated on the exfoliation of MoS_2 in this work, we believe the techniques described can be used to exfoliate a range of layered compounds. Thus, we hope this work opens the way to nanosheets production in a way that facilitates a broad spectrum of applications.

AUTHOR INFORMATION

Corresponding Author

*E-mail: colemaj@tcd.ie.

Notes

The authors declare no competing financial interest.

ACKNOWLEDGMENTS

The authors thank Science Foundation Ireland for financial support through the Principle Investigator scheme, grant number 07/IN.1/I1772 and the European Research Council grant SEMANTICS.

REFERENCES

(1) Geim, A. K. *Science* **2009**, *324*, 1530−1534.
(2) Wilson, J. A.; Yoffe, A. D. *Adv. Phys.* **1969**, *18*, 193−335.
(3) Novoselov, K. S.; Jiang, D.; Schedin, F.; Booth, T. J.; Khotkevich, V. V.; Morozov, S. V.; Geim, A. K. *Proc. Natl. Acad. Sci. U.S.A.* **2005**, *102*, 10451−10453.
(4) Alem, N.; Erni, R.; Kisielowski, C.; Rossell, M. D.; Gannett, W.; Zettl, A. *Phys. Rev. B* **2009**, *80*, 155425.
(5) Lee, C.; Yan, H.; Brus, L. E.; Heinz, T. F.; Hone, J.; Ryu, S. *Acs Nano* **2010**, *4*, 2695−2700.
(6) Mak, K. F.; Lee, C.; Hone, J.; Shan, J.; Heinz, T. F. *Phys. Rev. Lett.* **2010**, *105* (4), 136805.
(7) Splendiani, A.; Sun, L.; Zhang, Y. B.; Li, T. S.; Kim, J.; Chim, C. Y.; Galli, G.; Wang, F. *Nano Lett.* **2010**, *10*, 1271−1275.
(8) Bertolazzi, S.; Brivio, J.; Kis, A. *ACS Nano* **2011**, *5* (12), 9703−9.
(9) Radisavljevic, B.; Radenovic, A.; Brivio, J.; Giacometti, V.; Kis, A. *Nat. Nanotechnol.* **2011**, *6*, 147−150.
(10) Radisavljevic, B.; Whitwick, M. B.; Kis, A. *ACS Nano* **2011**, *5*, 9934−9938.
(11) Dean, C. R.; Young, A. F.; Meric, I.; Lee, C.; Wang, L.; Sorgenfrei, S.; Watanabe, K.; Taniguchi, T.; Kim, P.; Shepard, K. L.; Hone, J. *Nat. Nanotechnol.* **2010**, *5*, 722−726.
(12) Li, H.; Yin, Z.; He, Q.; Li, H.; Huang, X.; Lu, G.; Wen, D.; Fam, D. W. H.; Tok, A. L. Y.; Zhang, Q.; Zhang, H. *Small* **2011**, *8*, 63−67.
(13) Ayari, A.; Cobas, E.; Ogundadegbe, O.; Fuhrer, M. S. *J. Appl. Phys.* **2007**, *101*, 014507.
(14) Li, C.; Bando, Y.; Zhi, C. Y.; Huang, Y.; Golberg, D. *Nanotechnology* **2009**, *20* (6), 385707.
(15) Castellanos-Gomez, A.; Poot, M.; Steele, G. A.; van der Zant, H. S. J.; Agrait, N.; Rubio-Bollinger, G. *Adv. Mater.* **2012**, *24*, 772−775.
(16) Chang, K.; Chen, W. X. *J. Mater. Chem.* **2011**, *21*, 17175−17184.
(17) Chang, K.; Chen, W. X. *Chem. Commun.* **2011**, *47*, 4252−4254.
(18) Smith, R. J.; King, P. J.; Lotya, M.; Wirtz, C.; Khan, U.; De, S.; O'Neill, A.; Duesberg, G. S.; Grunlan, J. C.; Moriarty, G.; Chen, J.; Wang, J. Z.; Minett, A. I.; Nicolosi, V.; Coleman, J. N. *Adv. Mater.* **2011**, *23*, 3944−3948.
(19) Hu, Y.; Zhu, H. W.; Wang, J.; Chen, Z. X. *J. Alloys Compd.* **2011**, *509*, 10234−10240.
(20) Lee, K. M.; Song, M. S.; Kim, I. Y.; Kim, T. W.; Hwang, S. J. *Mater. Chem. Phys.* **2011**, *127*, 271−277.
(21) Zhang, J. T.; Jiang, J. W.; Zhao, X. S. *J. Phys. Chem. C* **2011**, *115*, 6448−6454.
(22) Coleman, J. N.; Lotya, M.; O'Neill, A.; Bergin, S. D.; King, P. J.; Khan, U.; Young, K.; Gaucher, A.; De, S.; Smith, R. J.; Shvets, I. V.; Arora, S. K.; Stanton, G.; Kim, H. Y.; Lee, K.; Kim, G. T.; Duesberg, G. S.; Hallam, T.; Boland, J. J.; Wang, J. J.; Donegan, J. F.; Grunlan, J. C.; Moriarty, G.; Shmeliov, A.; Nicholls, R. J.; Perkins, J. M.; Grieveson, E. M.; Theuwissen, K.; McComb, D. W.; Nellist, P. D.; Nicolosi, V. *Science* **2011**, *331*, 568−571.
(23) Hernandez, Y.; Nicolosi, V.; Lotya, M.; Blighe, F. M.; Sun, Z. Y.; De, S.; McGovern, I. T.; Holland, B.; Byrne, M.; Gun'ko, Y. K.; Boland, J. J.; Niraj, P.; Duesberg, G.; Krishnamurthy, S.; Goodhue, R.; Hutchison, J.; Scardaci, V.; Ferrari, A. C.; Coleman, J. N. *Nat. Nanotechnol.* **2008**, *3*, 563−568.
(24) Stankovich, S.; Dikin, D. A.; Dommett, G. H. B.; Kohlhaas, K. M.; Zimney, E. J.; Stach, E. A.; Piner, R. D.; Nguyen, S. T.; Ruoff, R. S. *Nature* **2006**, *442*, 282−286.
(25) Bissessur, R.; Heising, J.; Hirpo, W.; Kanatzidis, M. *Chem. Mater.* **1996**, *8*, 318−320.
(26) Joensen, P.; Frindt, R. F.; Morrison, S. R. *Mater. Res. Bull.* **1986**, *21*, 457−461.
(27) Osada, M.; Sasaki, T. *J. Mater. Chem.* **2009**, *19*, 2503−2511.
(28) Eda, G.; Yamaguchi, H.; Voiry, D.; Fujita, T.; Chen, M. W.; Chhowalla, M. *Nano Lett.* **2011**, *11*, 5111−5116.
(29) Zeng, Z. Y.; Yin, Z. Y.; Huang, X.; Li, H.; He, Q. Y.; Lu, G.; Boey, F.; Zhang, H. *Angew. Chem., Int. Ed.* **2011**, *50*, 11093−11097.
(30) Sandoval, S. J.; Yang, D.; Frindt, R. F.; Irwin, J. C. *Phys. Rev. B* **1991**, *44*, 3955−3962.
(31) Han, W. Q.; Wu, L. J.; Zhu, Y. M.; Watanabe, K.; Taniguchi, T. *Appl. Phys. Lett.* **2008**, *93*, 2889−2893.
(32) Lin, Y.; Williams, T. V.; Connell, J. W. *J. Phys. Chem. Lett.* **2010**, *1*, 277−283.
(33) Lin, Y.; Williams, T. V.; Xu, T. B.; Cao, W.; Elsayed-Ali, H. E.; Connell, J. W. *J. Phys. Chem. C* **2011**, *115*, 2679−2685.
(34) Warner, J. H.; Rummeli, M. H.; Bachmatiuk, A.; Buchner, B. *ACS Nano* **2010**, *4*, 1299−1304.
(35) Zhi, C. Y.; Bando, Y.; Tang, C. C.; Kuwahara, H.; Golberg, D. *Adv. Mater.* **2009**, *21*, 2889.
(36) Zhou, K. G.; Mao, N. N.; Wang, H. X.; Peng, Y.; Zhang, H. L. *Angew. Chem., Int. Ed.* **2011**, *50*, 10839−10842.
(37) Cunningham, G.; Lotya, M.; Cucinotta, C. S.; Sanvito, S.; Bergin, S. D.; Menzel, R.; Shaffer, M. S. P.; Coleman, J. N. *ACS Nano* **2012**, *6*, 3468−3480.
(38) Strano, M. S.; Moore, V. C.; Miller, M. K.; Allen, M. J.; Haroz, E. H.; Kittrell, C.; Hauge, R. H.; Smalley, R. E. *J. Nanosci. Nanotechnol.* **2003**, *3*, 81−86.
(39) Bergin, S. D.; Nicolosi, V.; Streich, P. V.; Giordani, S.; Sun, Z. Y.; Windle, A. H.; Ryan, P.; Niraj, N. P. P.; Wang, Z. T. T.; Carpenter, L.; Blau, W. J.; Boland, J. J.; Hamilton, J. P.; Coleman, J. N. *Adv. Mater.* **2008**, *20*, 1876−1881.
(40) Khan, U.; O'Neill, A.; Lotya, M.; De, S.; Coleman, J. N. *Small* **2010**, *6*, 864−871.
(41) O'Neill, A.; Khan, U.; Nirmalraj, P. N.; Boland, J.; Coleman, J. N. *J. Phys. Chem. C* **2011**, *115*, 5422−5428.
(42) Khan, U.; Porwal, H.; O'Neill, A.; Nawaz, K.; May, P.; Coleman, J. N. *Langmuir* **2011**, *27*, 9077−9082.
(43) Hennrich, F.; Krupke, R.; Arnold, K.; Rojas Stutz, J. A.; Lebedkin, S.; Koch, T.; Schimmel, T.; Kappes, M. M. *J. Phys. Chem. B* **2007**, *111*, 1932−1937.
(44) Lotya, M.; King, P. J.; Khan, U.; De, S.; Coleman, J. N. *ACS Nano* **2010**, *4*, 3155−3162.
(45) Lucas, A.; Zakri, C.; Maugey, M.; Pasquali, M.; van der Schoot, P.; Poulin, P. *J. Phys. Chem. C* **2009**, *113*, 20599−20605.
(46) Lee, C.; Wei, X. D.; Kysar, J. W.; Hone, J. *Science* **2008**, *321*, 385−388.
(47) Khan, U.; O'Neill, A.; Porwal, H.; May, P.; Nawaz, K.; Coleman, J. N. *Carbon* **2012**, *50*, 470−475.
(48) May, P.; Khan, U.; O'Neill, A.; Coleman, J. N. *J. Mater. Chem.* **2012**, *22*, 1278−1282.

(49) Nicolosi, V.; Vrbanic, D.; Mrzel, A.; McCauley, J.; O'Flaherty, S.; McGuinness, C.; Compagnini, G.; Mihailovic, D.; Blau, W. J.; Coleman, J. N. *J. Phys. Chem. B* **2005**, *109*, 7124−7133.
(50) Bergin, S. D.; Nicolosi, V.; Giordani, S.; de Gromard, A.; Carpenter, L.; Blau, W. J.; Coleman, J. N. *Nanotechnology* **2007**, 18.
(51) Giordani, S.; Bergin, S. D.; Nicolosi, V.; Lebedkin, S.; Kappes, M. M.; Blau, W. J.; Coleman, J. N. *J. Phys. Chem. B* **2006**, *110*, 15708−15718.
(52) Padawer, G. E.; Beecher, N. *Polym. Eng. Sci.* **1970**, *10*, 185−&.
(53) Blighe, F. M.; Young, K.; Vilatela, J. J.; Windle, A. H.; Kinloch, I. A.; Deng, L. B.; Young, R. J.; Coleman, J. N. *Adv. Funct. Mater.* **2011**, *21*, 364−371.
(54) Coleman, J. N.; Cadek, M.; Blake, R.; Nicolosi, V.; Ryan, K. P.; Belton, C.; Fonseca, A.; Nagy, J. B.; Gun'ko, Y. K.; Blau, W. J. *Adv. Funct. Mater.* **2004**, *14*, 791−798.
(55) Young, K.; Blighe, F. M.; Vilatela, J. J.; Windle, A. H.; Kinloch, I. A.; Deng, L. B.; Young, R. J.; Coleman, J. N. *ACS Nano* **2010**, *4*, 6989−6997.